KeAi

CHINESE ROOTS
GLOBAL IMPACT

Contents lists available at ScienceDirect

Petroleum Science

journal homepage: www.keaipublishing.com/en/journals/petroleum-science



Original Paper

Evolution of multi-cluster fracturing in high-density layered shale considering the effect of injection scheme



Xiao Yan ^a, Haitao Yu ^{b, c, *}, Peng Zhang ^d

- ^a School of Aerospace Engineering and Applied Mechanics, Tongji University, Shanghai, 200092, China
- ^b Department of Geotechnical Engineering, College of Civil Engineering, Tongji University, Shanghai, 200092, China
- ^c State Key Laboratory of Disaster Reduction in Civil Engineering, Tongji University, Shanghai, 200092, China
- ^d China Energy Technology and Economics Research Institute, Beijing, 102211, China

ARTICLE INFO

Article history: Received 16 July 2024 Received in revised form 6 March 2025 Accepted 6 March 2025 Available online 11 March 2025

Edited by Yan-Hua Sun

Keywords: Multi-cluster fracturing Bedding planes Fracture morphology Injection scheme Numerical simulation

ABSTRACT

Shale oil reservoir is generally characterized by well-developed bedding planes, and multi-cluster fracturing is the most effective technique to achieve stable shale oil production. In this paper, a multi-cluster fracturing model for a horizontal well in shale with high-density bedding planes is established. The fracture morphology, fracture geometry, fracturing area and multiple fracture propagation mechanism are analyzed under simultaneous fracturing, sequential fracturing, and alternative fracturing. Results show that in the case of small cluster spacing and three clusters, the growth of the middle fracture is inhibited and develops along the bedding planes under both simultaneous fracturing and alternative fracturing. For sequential fracturing, the increase in the interval time between each fracturing advances the post fracturing fracture deflecting to the pre-existing fractures through the bedding planes. The reactivation of the bedding planes can promote the extension of the fracturing area. Increasing the injection rate and the number of clusters promotes the activation of bedding planes. However, it is preferable to reduce the number of clusters to obtain more main fractures. Compared with modified alternating fracturing and cyclic alternating fracturing, alternating shut-in fracturing creates more main fractures towards the direction of the maximum in-situ stress. The fracturing efficiency for high-density layered shale is ranked as simultaneous fracturing > alternative fracturing > sequential fracturing. © 2025 The Authors. Publishing services by Elsevier B.V. on behalf of KeAi Communications Co. Ltd. This is an open access article under the CC BY-NC-ND license (http://creativecommons.org/licenses/by-nc-nd/ 4.0/).

1. Introduction

Shale oil development has obtained a worldwide concern with the continuous consumption of conventional energy. Geological exploration data illustrates that Sichuan Basin, Songliao Basin, Bohai Bay Basin, Ordos Basin, Junggar Basin, Santang Lake Basin, and Qaidam Basin, China, all have rich shale oil resources (Liu et al., 2019a, 2023b; Mei et al., 2023). Furthermore, the shale, as a typical sedimentary rock, generally has low permeability, low porosity, and well-developed bedding structures, in which the density of bedding planes ranges from milimeter to meter (Guo et al., 2023; Wei et al., 2023; Meng et al., 2024). Different from the exploitation of oil, shale gas, and coal, multi-stage and multi-cluster fracturing in horizontal wells is the most effective technique to achieve stable

shale oil production (Chang et al., 2022a). Previous theoretical results and experimental observation have proven that the bedding planes or natural fractures embed in the shale will affect the hydraulic fracture initiation and geometry (Blanton, 1982; Zhou et al., 2008; Cheng et al., 2014; Dahi Taleghani et al., 2016; Tan et al., 2017; Li, 2024; Pan et al., 2024). Thus, it is important to evaluate the multi-cluster fracturing characteristics in high-density layered shale and reasonably optimize the multi-cluster injection scheme for shale oil production.

Relevant studies have proved that the stress interference occurs due to the multi-cluster fracturing in horizontal wells, resulting in strong uneven expansion pattern of hydraulic fractures (Zangeneh et al., 2015; Siddhamshetty et al., 2018; Sobhaniaragh et al., 2018; Liu et al., 2019b; Dontsov and Suarez-Rivera, 2020). The number of perforation clusters and the fracture spacing are key factors controlling the stress interference and fracture morphology, with the closer fracture spacing strengthening the stress interference in one stage (Wu et al., 2016; Saberhosseini et al., 2019). Moreover, Tian

^{*} Corresponding author.

E-mail address: yuhaitao@tongji.edu.cn (H. Yu).

et al. (2019) established a multi-cluster hydraulic fracture propagation model using the extended finite element method, and proposed that the difference in geostress can offset the influence of stress interference between hydraulic fractures. Chen et al. (2020) found that the increased perforation number in cluster will promote the uniform fluid partitioning under high in-suit stress using a 3D planar multi-cluster fracturing model. Yang et al. (2018) emphasized that the reduction of fracturing fluid viscosity and the increase in injection rate will improve the uniformity of multicluster hydraulic fractures in a horizontal well. Li et al. (2018) studied the effect of perforation erosion on hydraulic fracture growth in multi-stage and multi-cluster hydraulic fracturing. Manchanda et al. (2017) found that not all clusters provide good and effective fracturing cracks, thus proposing an optimization scheme to adjust the cluster number to improve the stimulation. Wang et al. (2023) investigated the multiple fracture propagation path in large-angle oblique horizontal wells, revealing the impact of horizontal stress, injection rate, horizontal wellbore azimuth, and cluster spacing.

For the multiple fracture propagation under the influence of natural fractures or bedding planes, Ren et al. (2019) established two opposite natural fractures in the rock and analyzed the influence of stress anisotropy, layered distributed properties, and well deviation on anisotropy and heterogeneity of the propagation path of a two-cluster fracture system. Huang et al. (2022) conducted multi-cluster fracturing in shale reservoir and suggested that the complex hydraulic fracture network can be obtained by variable fluid-viscosity injection method. Liu et al. (2023c) found the shale anisotropy causes stronger stress interference on multiple hydraulic fractures. Qianli et al. (2023) developed a hydro-mechanical phase-field model to study the multi-cluster fracturing in discrete fracture network. Yang et al. (2022) applied coupled 3D displacement discontinuity method and finite volume method to analyze the fracture hydraulic morphology in fractured rock. They all discovered that the inter-cluster stress interference will be reduced effectively by activating natural fractures. However, few studies pay attention to the interaction of multi-cluster fracturing and bedding planes. Given the existence of high-density bedding planes in shale oil reservoir, the current research findings cannot effectively guide the shale oil production. The control mechanism of bedding on the fracturing behavior remains unclear.

The injection strategies also play an important role on fracturing efficiency. Chang et al. (2022b) conducted the experimental study in deep shale using constant fluid rate injection, cyclic injection, shut-in intermittent injection, and low-frequency pulse pressurization injection, finding that both the cyclic fracturing and shut-in fracturing can reduce the rock breakdown pressure, and pulse fracturing creates the most complex fracture morphology. Chang (2019) experimentally observed that the stepped-rise pump rate is conductive to opening the pre-existing discontinuity, while the cyclic-uplift injection method can only form a transverse fracture. Sesetty and Ghassemi (2013) pointed that the stress interference and the propagation of hydraulic fractures are both affected by fracturing sequence. Kumar and Ghassemi (2016) observed that sequential fracturing and modified alternative fracturing in a horizontal well could achieve greater fracture complexity. Wang et al. (2021) reported that the alternative fracturing scheme could generate better fracturing effect compared with sequential and simultaneous fracturing. Nevertheless, the fracturing efficiency in layered shale with different injection strategies still keeps a poor understanding.

In this paper, we use a novel unified pipe-interface element method (UP-IEM) proposed by Yan and his coworkers (Yan et al., 2021; Yan and Yu, 2022) to establish a multi-cluster fracturing model containing high-density bedding structure. The fracturing

efficiency of simultaneous injection, sequential injection, and alternative injection are investigated together with the fracture morphology, fracture geometry, and fracturing area. The paper is organized as follows: the methodology, numerical model, and numerical scheme are given in Section 2. In Section 3, we present the numerical results of multi-cluster simultaneous fracturing. The effect of cluster spacing, injection rate, and cluster number are discussed. In Section 4, fluid injection scheme including sequential fracturing and alternative fracturing are conducted. Also, the fracturing effect of modified alternating fracturing, alternating shut-in fracturing, and cyclic alternating fracturing are compared. The conclusions are drawn at the last section.

2. Mathematical model and numerical method

The numerical model in this study is calculated using the UP-IEM (Yan et al., 2021). In UP-IEM, the unified pipe network method (UPM) and the interface element (IE) are coupled to solve the hydro-mechanical coupled fracture propagation problem. The rock matrix is fully saturated. Compared with other existing methods or commercial software, UP-IEM is a simple yet accurate and robust numerical method to simulate fluid flow in discrete dual-permeability media. It is capable of capturing the overall anisotropy of the layered rock by explicitly representing bedding. The additional interchange term between bedding and surrounding rock is not needed as the interchange is already accounted for implicitly. In addition, it can consider both the cemented bedding and frictional bedding. The dilatation due to rough bedding surface during hydraulic fracturing is also calculated. Most previous studies only focus on the evolution of fracture parameters while ignoring the bedding plane evolution characteristics. The hydro-mechanical coupled mechanical equilibrium of the fractured rock is expressed based on the porelastic theory. The fluid flow in rock matrix, hydraulic fractures, and bedding planes follows Darcy's law. The UP-IEM has been successfully applied in modeling seepage and hydraulic fracturing on a laboratory scale and field scale (Sun et al., 2019; Yan and Yu, 2022; Yan et al., 2021, 2024).

2.1. Basic equations

2.1.1. Fluid flow equation

The fluid flow in both perforation clusters and fractured rock is governed by Darcy's law, and the mass conservation equation is expressed as follows (Rutqvist et al., 2002; Shao et al., 2024):

$$\rho_{w}S\frac{\partial p}{\partial t} + \alpha\rho_{w}\frac{\partial \varepsilon_{vol}}{\partial t} + \nabla\left(\rho_{w}\frac{1}{\eta}k\nabla p\right) = \rho_{w}q_{s} \tag{1}$$

where ρ represents the fluid density; S is the specific storage; p is fluid pressure; α is the Biot coefficient; ε_{vol} is the volumetric strain; η represents the fluid viscosity; k represents the permeability; and q_s is the source term.

2.1.2. Equilibrium equation

The hydro-mechanical coupling is expressed according to the change of effective stress. The Biot coefficient α is used to express the influence of fluid pressure as follows:

$$\nabla(\boldsymbol{\sigma}' - \alpha p \boldsymbol{I}) = 0 \tag{2}$$

where σ' is the effective stress tensor; and I is the identity tensor.

2.1.3. Fracture propagation equation

The cohesive-frictional zone model proposed by Barenblatt (1962) is used to describe the hydraulic fracture propagation. The

relationship between cohesive traction and separation is determined by a linear softening law (Snozzi and Molinari, 2013):

$$\boldsymbol{t}_{\mathrm{d}} = \frac{\overline{t}}{u} \left(u_{\mathrm{N}} + \frac{\beta^2}{\kappa} u_{\mathrm{T}} \right) \tag{3}$$

$$u = \sqrt{u_{\rm N}^2 + \frac{\beta^2}{\kappa^2} u_{\rm T}^2} \tag{4}$$

where t_d is the cohesive traction; \bar{t} is an equivalent traction; u is the equivalent fracture opening; u_N and u_T represents the normal and tangential separation over the surface. The parameter β accounts for the ratio of tensile strength to shear strength, the parameters κ defines the ratio between the fracture energy in Mode-II and Mode-I.

2.1.4. Slip equation

The frictional slip and stick behavior of the bedding planes are controlled by classical Coulomb's friction law (Oliver et al., 2008):

$$u_{\rm N} \ge 0, \ t_{\rm N}^{\rm c} \le 0, \ u_{\rm N} \cdot t_{\rm N}^{\rm c} = 0$$
 (5)

$$f = \left\| t_{\mathrm{T}}^{\mathrm{f}} \right\| - \left\| \mu \cdot t_{\mathrm{N}}^{\mathrm{c}} \right\| \begin{cases} = 0, \text{ slipping} \\ < 0, \text{ sticking} \end{cases}$$
 (6)

where $t_{\rm N}^{\rm c}$ is the normal closure traction; $t_{\rm T}^{\rm f}$ is the tangential frictional traction; and μ is Coulomb's friction coefficient. When the shear stress is less than the bedding strength (defined as $\mu \cdot t_{\rm N}^{\rm c}$), a stick situation governs the relative displacement of the discontinuities, while a slip situation is restricted to the value once the shear stress is equal to the bedding strength.

2.1.5. Aperture evolution equation

The permeability of the hydraulic fractures and bedding planes is written based on the evolution of aperture (*w*) (Witherspoon et al., 1980):

$$k = \frac{w^2}{12} \tag{7}$$

The generation of hydraulic fracture is considered as tensile failure, thus the aperture of the hydraulic fracture is obtained directly according to the normal separation. While for the bedding planes, the aperture varies under compressive load and tensile load. The aperture for hydraulic fractures and bedding planes can be written as follows (Saeb and Amadei, 1992; Rutqvist et al., 2002; Fang et al., 2017; Nguyen et al., 2017):

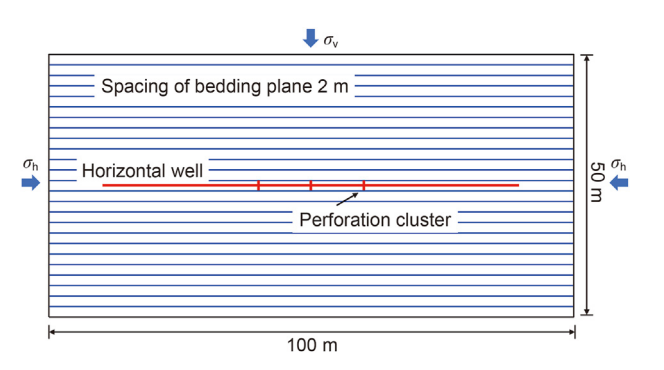


Fig. 1. Diagram of a numerical model for hydraulic fracturing of shale specimen.

2.2. Numerical model

As shown in Fig. 1, a numerical model with a width of 100 m and a height of 50 m containing high-density bedding planes is established. Due to the density of bedding planes ranging from millimeter to meter in shale oil reservoir (Guo et al., 2023; Wei et al., 2023; Meng et al., 2024), the spacing of the bedding plane is defined as 2 m. The vertical stress $\sigma_{\rm V}=40$ MPa is loaded on the top edge of the model domain, as well as the minimum horizontal stress $\sigma_h = 25$ MPa is acted on the right and left boundaries of the model. The normal displacement of the bottom edge is fixed. A horizontal well is located in the middle of the model with several clusters. In this study, the basic mechanical and hydraulic parameters for the simulation are obtained from the shale oil reservoir in Jiyang Depression, Bohai Bay Basin, Eastern China, which was tested using laboratory experiments by (Liu et al., 2023a; Li et al., 2024). In their experiments, the permeability of the rock matrix ranges from 5×10^{-18} to 2×10^{-15} m². The intrinsic permeability in this study is assumed to be low-permeable with 1×10^{-17} m². The mechanical and fluid parameters are listed in Table 1.

In this study, simultaneous fracturing, sequential fracturing, and alternative fracturing are conduced to estimate the evolution of multi-cluster fracturing. In single-stage multi-cluster simultaneous fracturing simulation, the effect of different cluster spacing, injection rate, and cluster number are discussed, as presented in Fig. 2(a). In the multi-cluster sequential fracturing, three fracturing clusters are modeled in one stage with different interval time (Fig. 2(b)). In the multi-cluster alternative fracturing, to compare with the sequential fracturing, we firstly conduct a three-cluster fracturing with different interval time, in which the middle cluster is injected at last with the continuous injection for Cluster 1, Cluster 2, and Cluster 3 (see Fig. 2(c)). After that, we design three

$$w = \begin{cases} u_{\text{N}}, \text{ hydraulic fractures} \\ w_{\text{r}} + (w_0 - w_{\text{r}}) \exp\left(-\frac{1}{K_{\text{n}}(w_0 - w_{\text{r}})} t_{\text{N}}^{\text{c}}\right) + \Delta u_{\text{T}} \tan \psi, \text{ bedding planes (compressive load)} \\ w_0 + u_{\text{N}}, \text{ bedding planes (tensile load)} \end{cases}$$
(8)

where w_r represents the residual aperture; w_0 represents initial aperture under zero stress; K_n represents the stiffness of the bedding planes; and ψ represents the dilation angle.

different alternative injection schemes under nine perforations with two stages (Xia et al., 2024), as displayed in Fig. 2(d). In the first scheme, the fluid is firstly injected into Cluster 1 and then injected into Cluster 2, called the modified alternating fracturing (Fig. 3(a)). The second scheme is an alternating shut-in fracturing with a shut-in period existing between the fracturing of Cluster 1

 Table 1

 Input material parameters for numerical simulation.

Parameter	Value
Young's modulus E, GPa	20
Poisson's ratio v	0.22
Biot coefficient a	1
Initial porosity $\phi_0^{\rm m}$	0.02
Intrinsic permeability k , m^2	1×10^{-17}
Fracture energy G_f , N/m	51
Tensile strength f_t , MPa	2.0
Scaling factor for rock strength β	1
Scaling factor for fracture energy κ	1
Stiffness of bedding plane K_n , GPa/m	200
Initial aperture of bedding planes w_0 , mm	0.01
Residual aperture of bedding planes w_r , mm	0.001
Friction coefficient μ	0.4
Dilation angle ψ , $^\circ$	10
Fluid viscosity η , Pa s	0.001
Fluid density $\rho_{\rm w}$, kg/m ³	1000
Injection rate q , m^2/s	1×10^{-4}

and Cluster 2 (Fig. 3(b)). The last scheme is a cyclic alternating fracturing (Fig. 3(c)). In these schemes, the injection rate q_1 associated with Cluster 1 and q_2 with Cluster 2 (Xia et al., 2024).

3. Simultaneous fracturing

In this section, to study the effect of key multi-cluster fracturing factors on multiple hydraulic fracturing, we analyze the fracture propagation path, fracture geometry, and fracturing area.

3.1. Effect of cluster spacing

Previous work of multi-cluster fracturing in homogeneous rock found that a small cluster spacing will strength the stress interference and further affect the fracture morphology. However, the impact of cluster spacing on multiple fracture propagation behavior and fracturing efficiency in shale with high-density bedding planes is still not clear. In this section, three fractures propagate

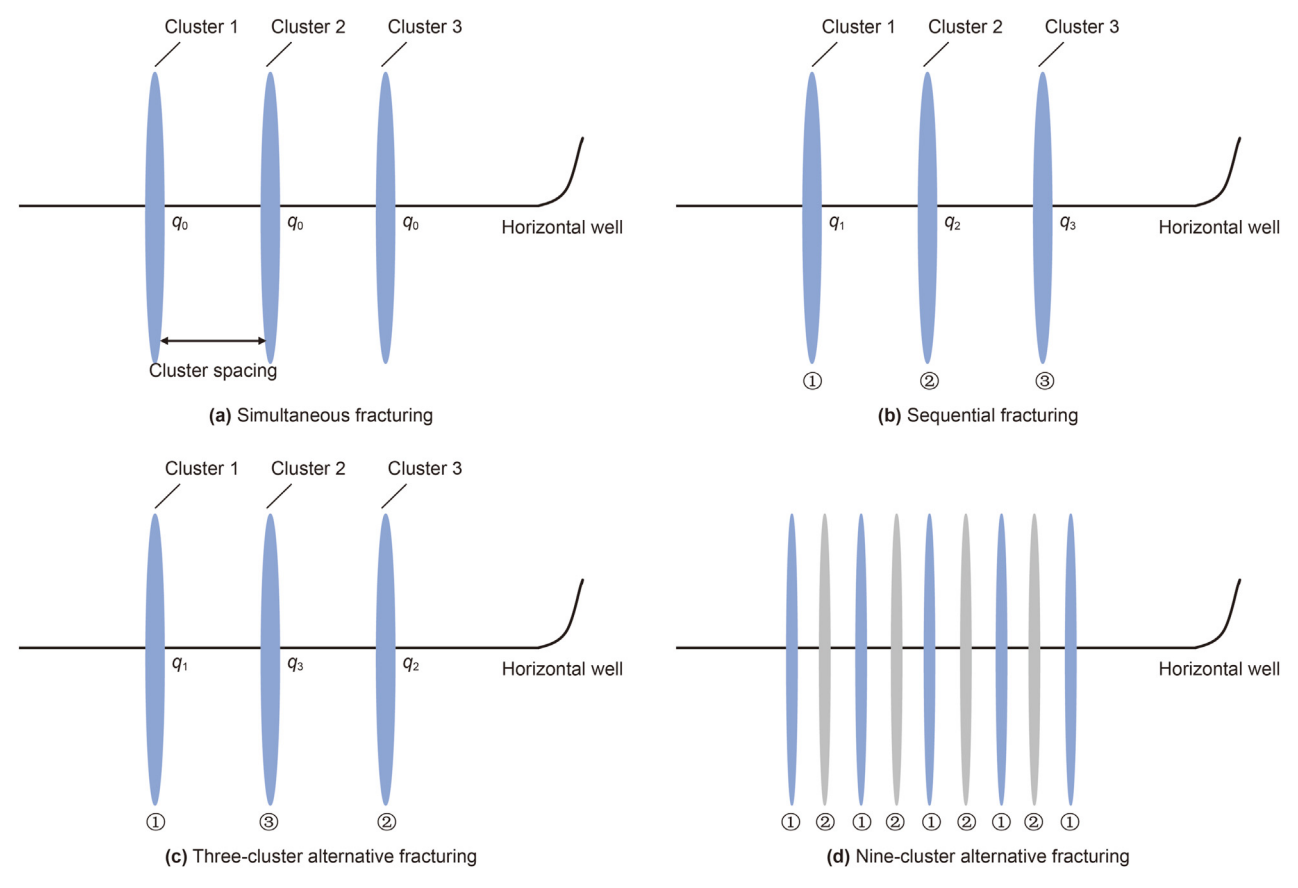


Fig. 2. Injection schemes for multi-cluster fracturing in a horizontal well.

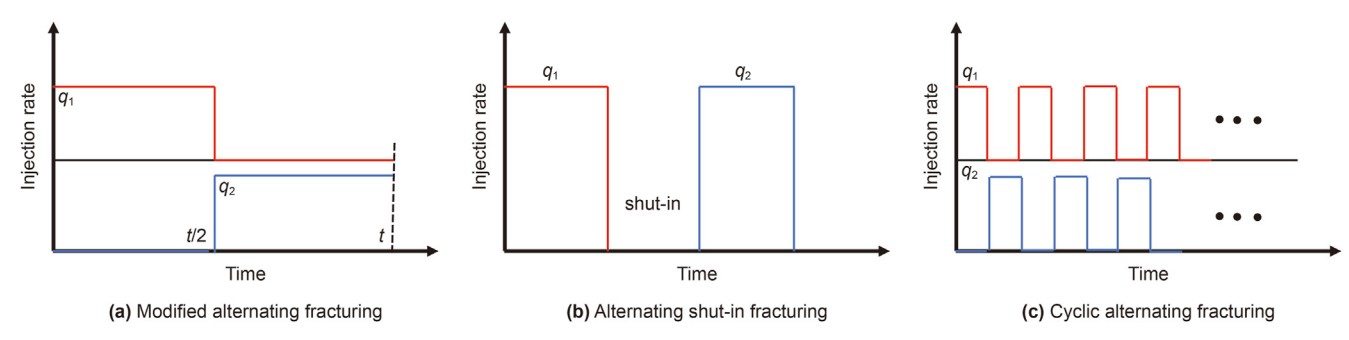


Fig. 3. Three kinds of alternative injection schemes under nine-cluster fracturing process.

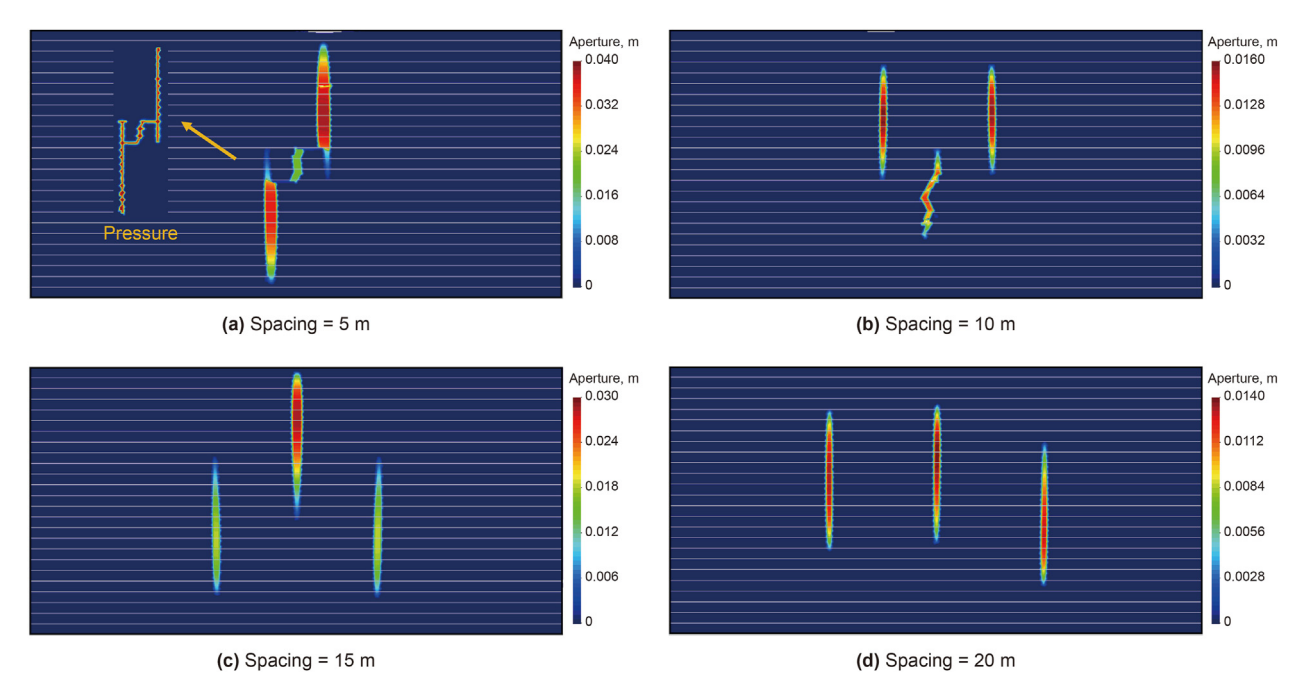


Fig. 4. Three-cluster fracture propagation behavior under different cluster spacing.

simultaneously with fracture spacing of 5, 10, 15 and 20 m, respectively.

Fig. 4 shows three-cluster fracture propagation behavior under different cluster spacing. When the cluster spacing is 5 m, the middle fracture (Cluster 2) will cross two layers of bedding planes and then be arrested. The upper part of the left fracture (Cluster 1) and the bottom part of the right fracture (Cluster 3) are compressed by the middle fracture, causing uneven fracture width along the hydraulic fracture length. It can also be observed from the pore pressure contour as shown in Fig. 4(a), the fracturing fluid penetrates into the bedding planes, while the aperture of the bedding planes is smaller compared with the hydraulic fractures. The slippage of the bedding planes has a non-negligible influence on hydraulic fracturing. For larger cluster spacing, the influence of bedding planes and stress interference on the propagation path of hydraulic fracture is weakened, which is similar as the results in previous studies (Yang et al., 2018; Ma et al., 2022). Especially when the cluster spacing is 20 m, the three fractures propagate more independently towards the vertical stress, as well as the fracture apertures along the propagation path are almost the same. Different from the multi-cluster fracturing results in intact rock, it was noticed that hydraulic fractures could bypass the inter-cluster interference by connecting bedding planes. The existence of bedding planes would induce the middle fracture to be arrested or results in the fracture merging and diverting.

Fig. 5 presents the variations of fracture aperture with time at the inlet position for different cluster spacing. In the initial propagation stage, the width of the three fractures at the inlet position all increases gradually with the continuous injection and the aperture difference is minor. This is because the stress shadow between the hydraulic fractures is small and the stress conditions at fracture tips are analogous. However, when the cluster spacing is small, the propagation of single cluster fracture will result in an intense compressive load on the rock matrix and leads to a closure of the existing hydraulic fractures. For cluster spacing of 5 m, the edge fractures at the inlet position are squeezed by the middle fracture, and it is predicted that the aperture will decreases continuously. Nevertheless, the slippage of the bedding planes

promotes a further expansion on hydraulic fracture aperture after the bedding plane is activated and connected with the outer cluster fractures. This phenomenon could be observed in Fig. 5, after the bedding plane is activated and connected at approximately 80 s, the fracture width further shows an obviously increase trend. On the contrary, with the increase in cluster spacing, no bedding is activated, and the fracture width for three-cluster fractures is almost the same, indicating that the fracture is more likely to growth like single fracture (Fig. 5).

Due to the shale oil may exist in the bedding planes, it is necessary to consider the reactivation area of the bedding planes. Thus, the fracturing area in the current study includes the artificial fracture area and the reactivated bedding plane area. Note that the artificial fracture area here is determined as the accumulation of the fracture area in each cracked element which is the product of fracture height and fracture aperture. The reactivated bedding plane area is defined as the product of bedding plane opening (normal width and dilation width) and bedding length. The fracturing area under different cluster spacing is shown in Fig. 6. The fracturing area is the largest when the cluster spacing is 5 m, and an obvious growth is found when the fracturing time is about 90 s. The results mean that the activation of the bedding planes together with the connection between the hydraulic fractures and bedding planes could promote the fracturing efficiency.

3.2. Effect of injection rate

The injection rate plays an important role on pore pressure distribution, the interaction between hydraulic fractures and natural fractures, as well as hydraulic fracture geometry (Remij et al., 2015; Khisamitov and Meschke, 2021; Yan and Yu, 2022). This section chooses four different injection rates to investigate the three-cluster fracture propagation pattern in bedding planes. The injection rates in each cluster are 2×10^{-5} , 1×10^{-4} , 2×10^{-4} , and 3×10^{-4} m²/s. The cluster spacing is 5 m.

As for the fracture propagation path and aperture distribution shown in Fig. 7, its variation strongly depends on fracturing fluid injection rate. With a low injection rate, the fluid tends to flow into

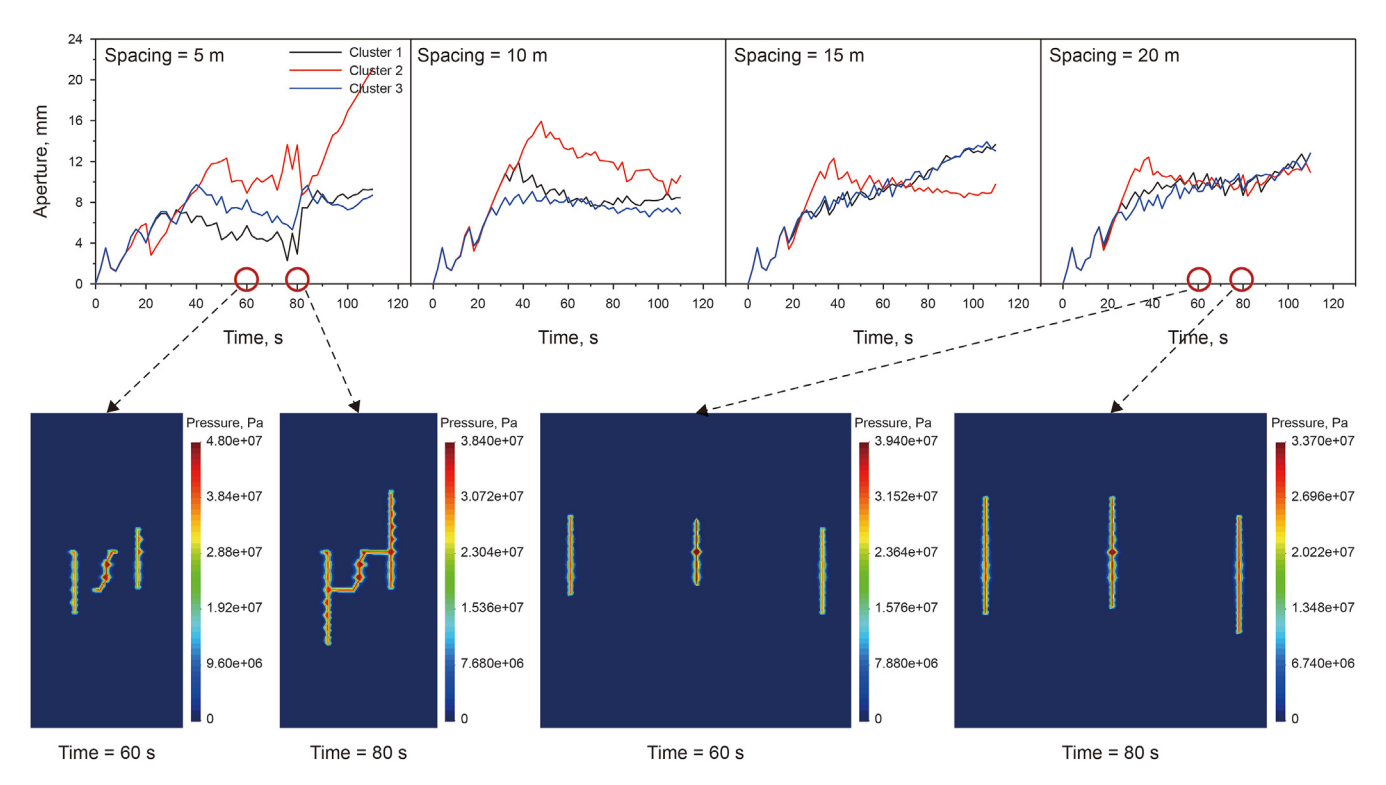


Fig. 5. Variations of fracture aperture with time at the inlet position for different cluster spacing.

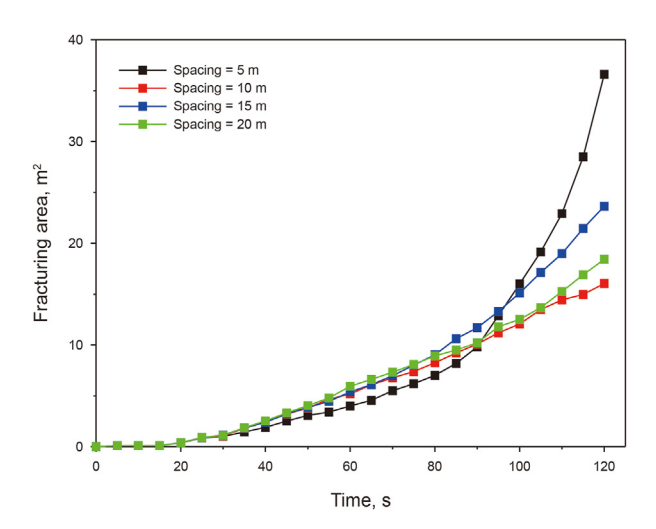


Fig. 6. Variations of fracturing area with time for different cluster spacing.

the bedding planes, and it is difficult for main fractures to wake bedding planes so as to induce shear slip of bedding planes. For the case $q=2\times 10^{-5}~\text{m}^2/\text{s}$, all fractures develop along the bedding planes. It is noted that the middle fracture initially propagates vertically crossing several bedding planes and then tends to deflect to the left fracture and right fracture through the bedding planes when $q=1\times 10^{-4}~\text{m}^2/\text{s}$ and $q=2\times 10^{-4}~\text{m}^2/\text{s}$. Once the hydraulic fracture deflects along the bedding planes, approaching hydraulic fractures initially induce shearing along bedding planes. When the injection rate is further increased to $q=3\times 10^{-4}~\text{m}^2/\text{s}$, the three-cluster fractures mainly extend crossing the bedding planes. Combined Figs. 7 and 8, a larger stress shadow (σ_{XX}) and fluid pressure disturbance caused by high injection rate are easier to induce the middle fracture deflection.

The previous simulation results prove that under the small cluster spacing, the middle fracture is restricted to propagate due to the stress interference under low injection rate. Fig. 9 illustrates the evolution curves of fracture aperture at injection points. As seen, the total fracture width increases gradually with injection rate. Increasing fluid flow rate increases shear displacement at the junction of hydraulic fractures with bedding planes. The shearing displacement and dilation further promote the aperture of the hydraulic fractures. According to the comparison results of fracturing area considering the influence of injection rate during threecluster fracturing (Fig. 10(a)), under the same fracturing time, the total fracture area shows an increasing trend as the increase in the injection rate. However, the fluid injection volume also acts as a dominant factor influencing the fracturing behavior. Fig. 10(b) presents the relationship between fracturing area and total injection volume. It is also found that although the gradual increase in pumping rate can effectively increase the width of the fracture system and promote the fracturing area, attention still needs to be paid to the competing factors of fluid volume, as well as the activation of bedding planes. Increasing the injection rate is conducive to generate vertical main fractures.

3.3. Effect of the number of clusters

The main parameters in layout of the multi-cluster perforation include the number of clusters and the cluster spacing. The key problem still needed to be addressed is whether the transformation efficiency of the shale reservoir with high-density bedding planes could be enhanced by increasing the number of clusters. Four cases with cluster number of 3, 5, 7 and 9 are considered. The cluster spacing is defined as 5 m. Two schemes are conducted here, in which Scheme 1: The injection rate in each cluster is $1\times 10^{-4}~\text{m}^2/\text{s}$. Scheme 2: The total injection rate is fixed as $9\times 10^{-4}~\text{m}^2/\text{s}$ in the horizontal well.

Figs. 11 and 12 show the comparison of different fracture

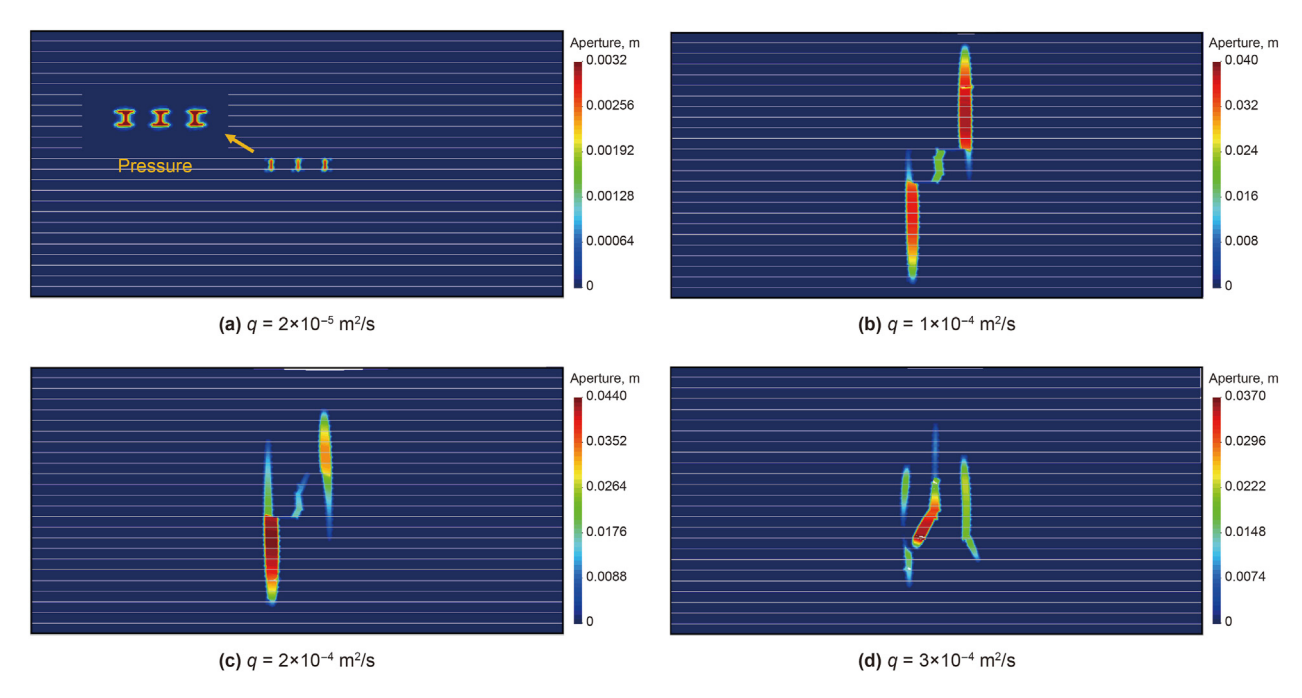


Fig. 7. Three-cluster fracture propagation behavior under different injection rates.

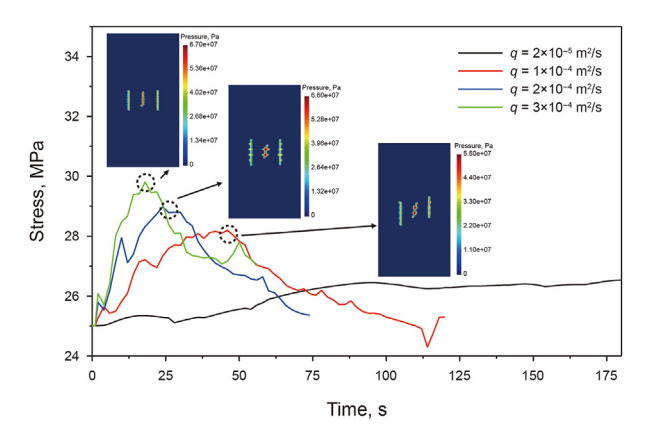


Fig. 8. Variations of stress with time at the middle point between Cluster 1 and Cluster 2 (The dashed line circle means that the middle fracture starts to deflect to the edge fractures.).

network patterns under different number of clusters. As seen, with the increase in the number of clusters, bedding planes are easier to be activated and the inter-cluster hydraulic fractures are more likely to be arrested by the bedding planes. The multiple fractures present intense competition propagation phenomenon with continuous fluid injection. More interior cluster fracture propagation will be impeded by the bedding planes with the increased number of clusters. The growth rate of the artificial main fracture becomes slow affected by the activated bedding planes. The injection fluid accumulates in the connected multiple fractures and promotes their aperture. For the constant total injection rate, the three-cluster hydraulic fractures could initiate effectively and cross the bedding planes, eventually, these fractures merge together in the rock matrix and propagate forward. This is because the intense fluid pressure in each cluster promotes the effective initiation and propagation.

Fig. 13 illustrates the evolution of fracturing area for four cases with different numbers of clusters. It is worth mentioning when the total injection rate is fixed, the fracturing area with the cluster number of 5 and 7 is almost the same. The competition among more cluster fractures restricts the fracturing transformation. In addition, the number of the failure elements (includes the elements representing the hydraulic fracture and the elements representing the activating bedding) does not satisfy the similar increasing mode. More clusters increase the probability of hydraulic fractures communicating with bedding planes to obtain more failure

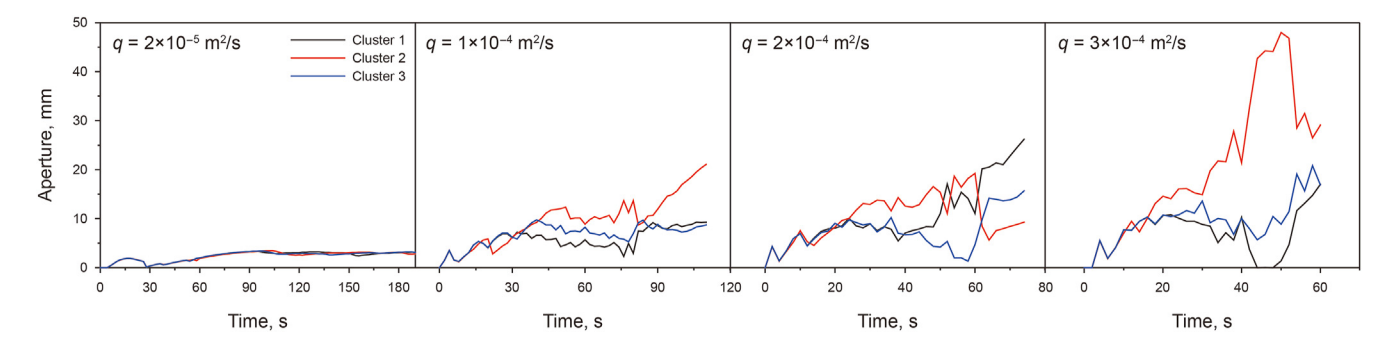


Fig. 9. Variations of fracture aperture with time at the inlet position for different injection rates.

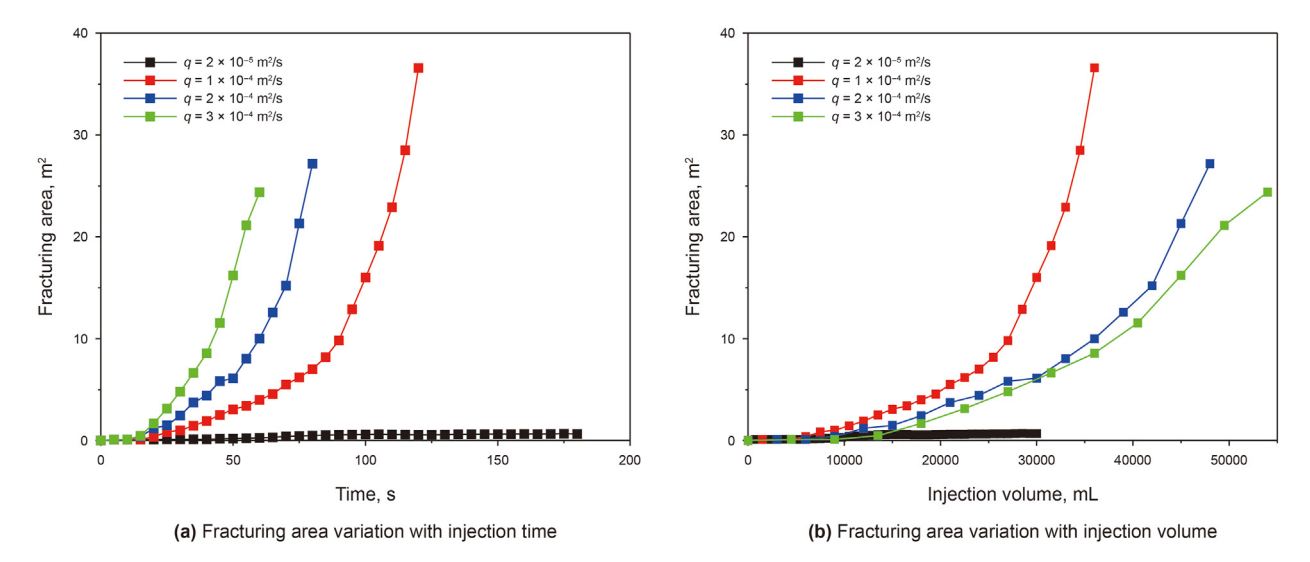


Fig. 10. Variations of fracturing area with time and injection volume at different injection rates.

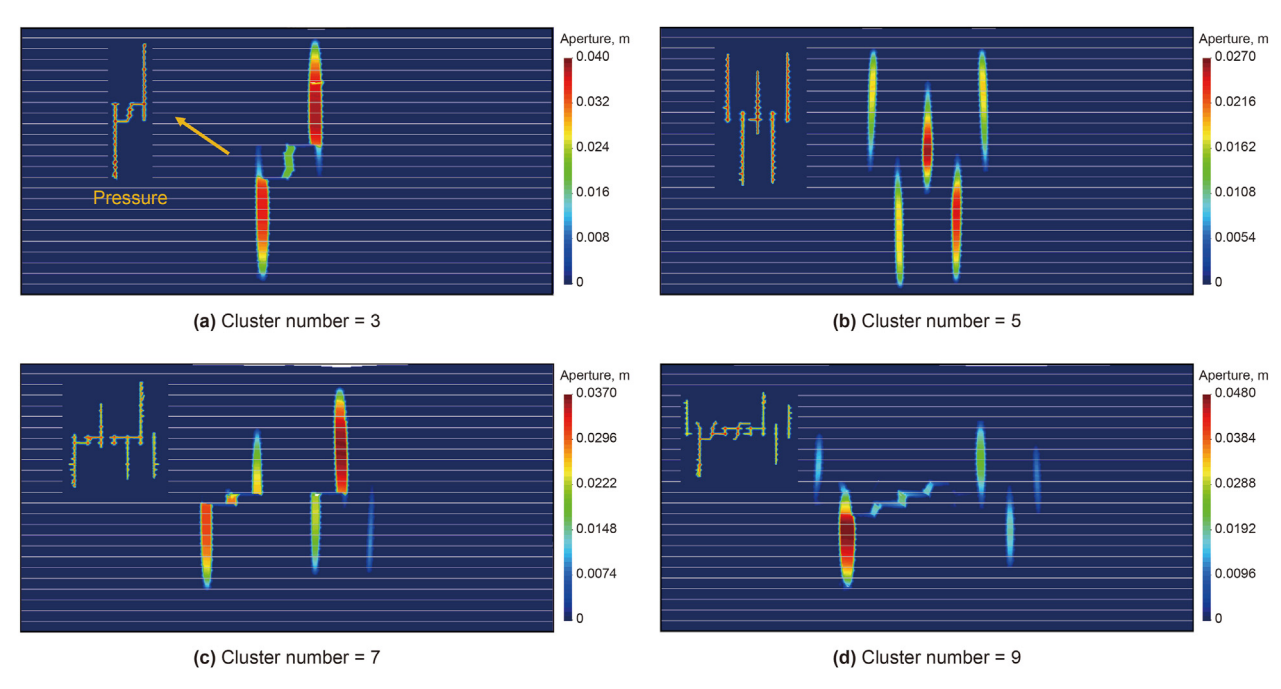


Fig. 11. Multi-cluster fracturing behavior under different numbers of clusters with the injection rate of 1×10^{-4} m²/s in each cluster.

elements, but the competition flow distribution may cause an unsatisfactory stimulation response. Considering the existence of shale oil in the bedding planes, comprehensively balancing the fracturing area and bedding plane activation area, relatively small cluster number with a closely spaced stage may more profitable to fractured shale stimulation.

4. Sequential fracturing and alternative fracturing

Multi-cluster sequential fracturing and alternative fracturing are also important injection scheme usually used in the actual oil and gas production. Influenced by the stress redistribution and non-uniform pore pressure induced by fracturing (Yan and Yu, 2022), the time interval and injection sequence of each cluster will have non-negligible effect on multiple fracturing behavior. The injection scheme conducted in this section is given in Fig. 2.

4.1. Effect of time interval between each fracturing

To discuss the effect of time interval and injection sequence on multi-cluster fracturing with bedding planes, two kinds of cases are designed here, as shown in Fig. 2. (1) Sequential fracturing: fracturing fluid is firstly injected into Cluster 1, and then followed by Cluster 2 and Cluster 3. (2) Alternative fracturing: fracturing fluid is still firstly injected into Cluster 1, however, Cluster 3 is injected earlier than Cluster 2. The time interval between each fracturing is chosen as 10, 20, 30, and 40 s, respectively. The cluster spacing is 5 m. The injection rate in each cluster is kept as 1×10^{-4} m²/s.

According to the results of three-cluster fracture propagation for fracturing sequence Cluster 1 - Cluster 2 - Cluster 3 as shown in Fig. 14, we observe that the new hydraulic fracture is easier to deflect towards the existed fractures with the increase in the interval time between each fracturing. When the time interval $\Delta t = 10$ s, the left

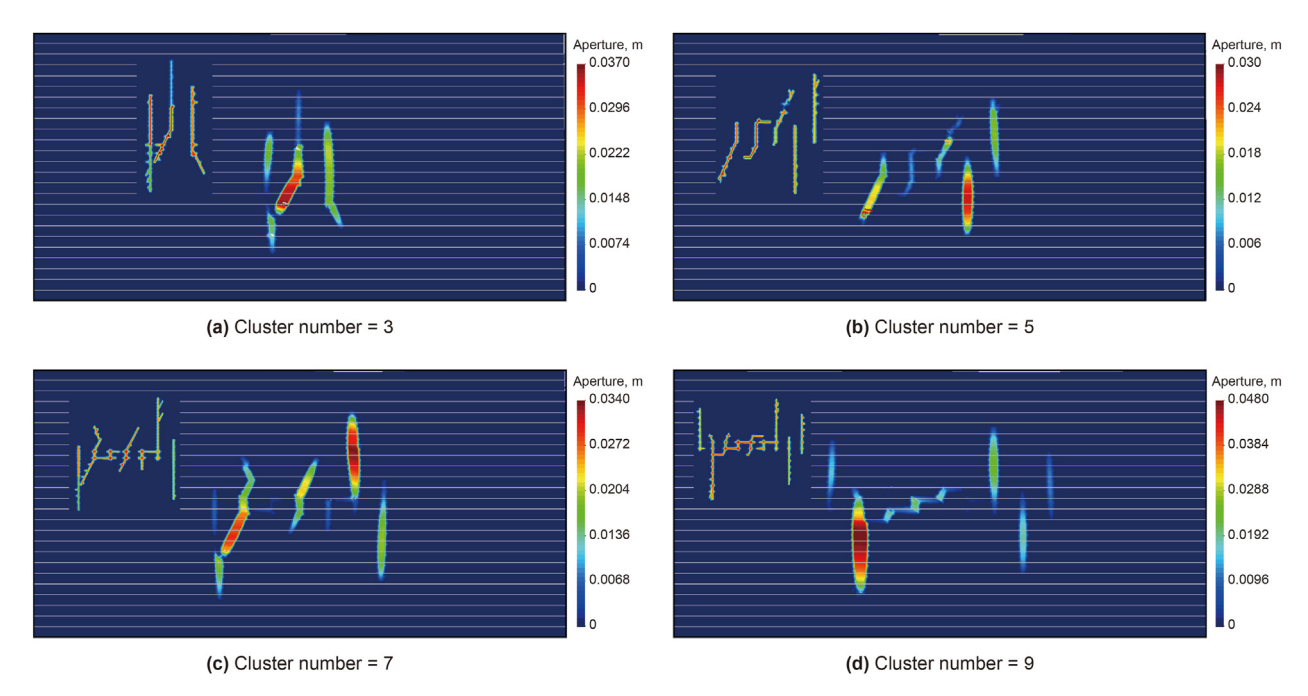


Fig. 12. Multi-cluster fracturing behavior under different cluster numbers with the total injection rate of 9×10^{-4} m²/s.

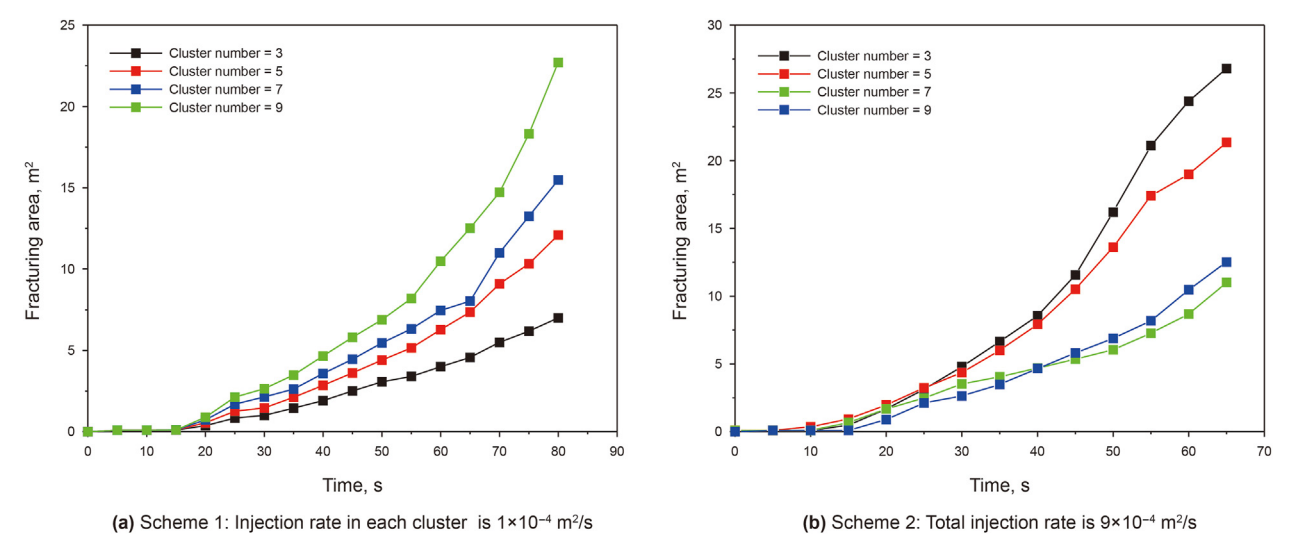


Fig. 13. Variations of fracturing area with time for different cluster numbers.

and middle fractures propagate perpendicular to the bedding planes, while the right fracture is partly arrested by the bedding planes. For the time interval $\Delta t = 20$ s and 30 s, the bottom of the middle fracture turns to the left fracture and the right fracture develops along the bedding planes. When the time interval $\Delta t = 40$ s, the three-cluster fractures are connected by the bedding planes. The bedding planes will be reactivated accompanying the opening and slipping after the second and third cluster fracturing. The early fracturing causes a more obvious stress interference and nonuniform pore pressure on the subsequent fracturing than the simultaneous fracturing. The non-uniformly distributed aperture on hydraulic fractures explains the interaction between different cluster fracturing. It is also noted that the preferential propagated fracture presents a smaller aperture before connecting with the activated bedding planes. The slipping and dilation of bedding planes restrict the vertical development of the subsequent fractures.

Fig. 15 presents the fracture aperture variation at the injection point for fracturing sequence Cluster 1 - Cluster 2 - Cluster 3. For the time interval of 10, 20, and 30 s, the aperture of the middle fracture is always larger than the other two fractures, which is because a higher pressure is needed to push the middle fracture initiation by resisting the stress interference induced by the first cluster fracturing, and then causes a larger opening of the hydraulic fracture. The right fracture generally has the smallest aperture due to the hydraulic fracture arrested by the bedding plane with the bedding planes activating. Fig. 15 also shows that the aperture of the middle aperture increases sharply at the later period of fracturing when the time interval is 10, 20 and 30 s, while a sudden drop is observed for the left fracture when $\Delta t = 40$ s. It can be speculated that an obvious growth of previous cluster fracture aperture occurs once the fracturing fluid penetrates into the connected previous cluster fracture. When Cluster 2 fracture and

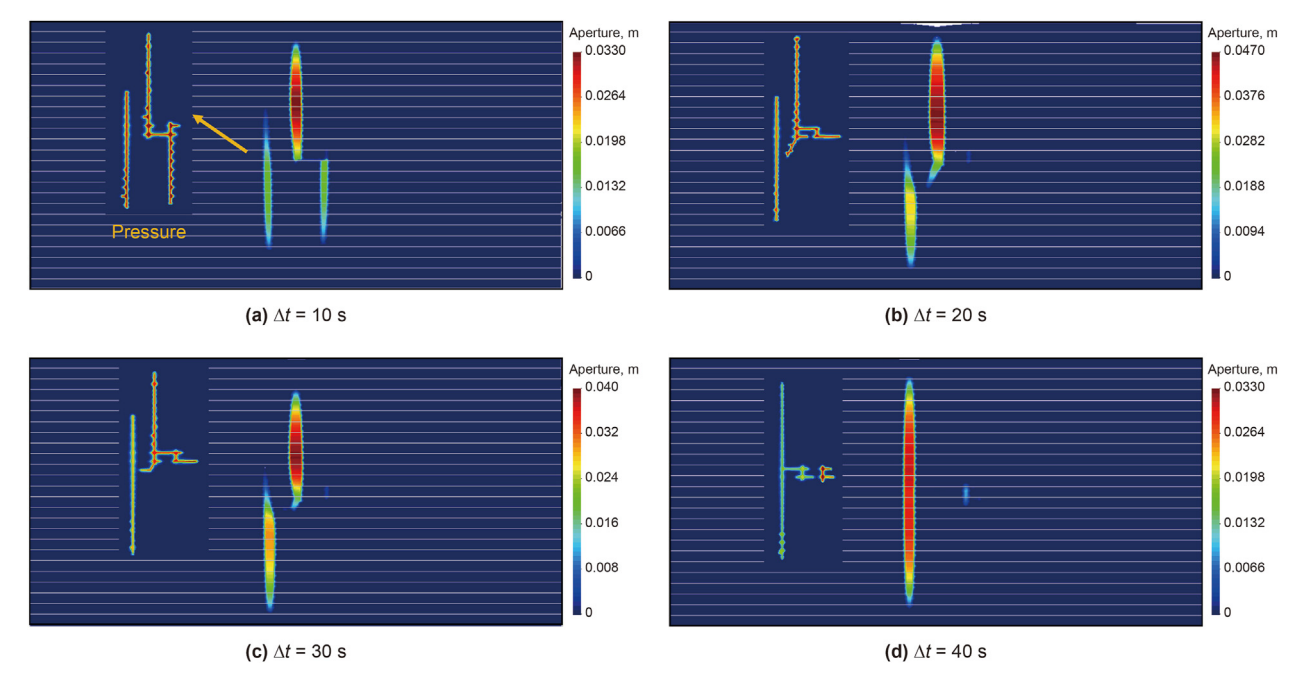


Fig. 14. Three-cluster fracture propagation behavior for fracturing sequence: Cluster 1 - Cluster 2 - Cluster 3.

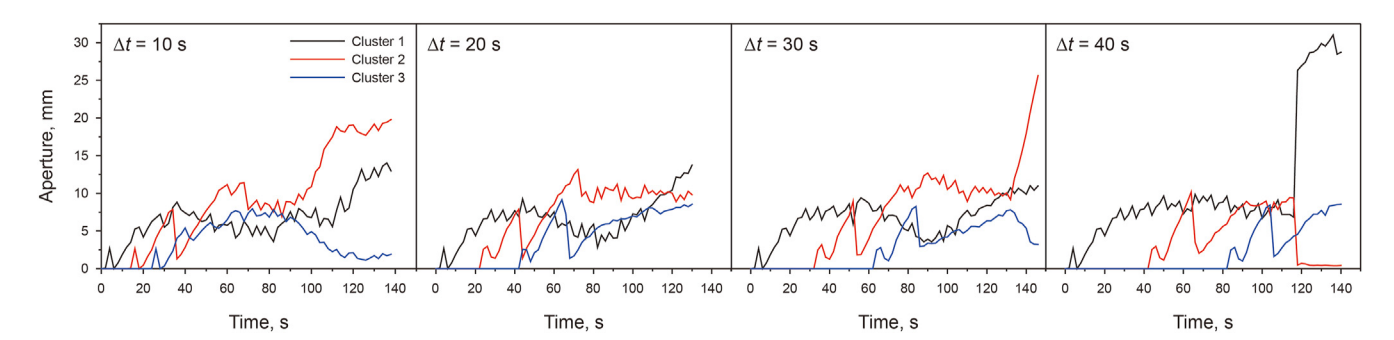


Fig. 15. Variations of fracture aperture with time for fracturing sequence: Cluster 1 - Cluster 2 - Cluster 3.

Cluster 3 fracture develop along the bedding planes, more fluid accumulates in Cluster 1, and the compressive load around Cluster 2 causes a sharp decrease in aperture for Cluster 2.

Fig. 16 shows the crack morphology for alternative fracturing with fracturing sequence Cluster 1 - Cluster 3 - Cluster 2. The middle fracture is strongly affected by the previous cluster fracturing. Also, the increase in the interval time between each fracturing results in a larger stress shadow effect on the neighborhood fracture. Although a larger injection pressure for the middle cluster fracturing may be required, the activation of the bedding plane cannot promote a long and wide single fracture. On the contrast, a connected and complex fracture network may be generated. The last cluster fracture generally has the minimum aperture due to the existence of the bedding planes. As observed in the evolution curve of the fracture aperture at the injection point (see Fig. 17), the right fracture and the left fracture display the similar variation trend during the fracturing process. The quick growth of Cluster 1 and Cluster 3 fractures generates obvious compressive load around Cluster 2, thus resulting in a sudden drop in aperture for Cluster 2.

The fractures generated in the first cluster are open, with the increase in interval time, the rock matrix is squeezed. In addition, the fluid pressure mainly accumulates in the previous fractures. The pre-fracturing obviously affects the stress distribution and pore

pressure field. Yan and Yu (2022) proposed that the hydraulic fractures are more likely to coalesce with existing fracture branches, the expansion of hydraulic fractures is highly influenced by the macroscopic gradient distribution of pore pressure. Thus, the increase in interval time will lead to a worse fracturing effect of the post-fracturing. Especially arrested by the bedding planes, the post-fracturing crack is difficult to grow in the vertical direction with the increase in interval time.

The fracturing area decreases with the interval time increasing for different multi-cluster fracturing sequences, as shown in Figs. 18 and 19. For fracturing sequence Cluster 1 - Cluster 2 - Cluster 3, it is noted that although the number of the damaged elements is the least for interval time of 40 s, the aperture of the main fracture and the slipping displacement of bedding planes are larger, resulting in the fracturing area larger. It could be predicted that, choosing a relatively long time interval is suitable to efficiently activate the bedding plane, while more main fractures will be obtained at a small interval time. For alternative fracturing Cluster 1 - Cluster 3 - Cluster 2, the fracturing morphology is almost the same. Compared Figs. 18 and 19, the alternative fracturing could have a better fracturing efficiency than the sequential fracturing under the three-cluster fracturing.

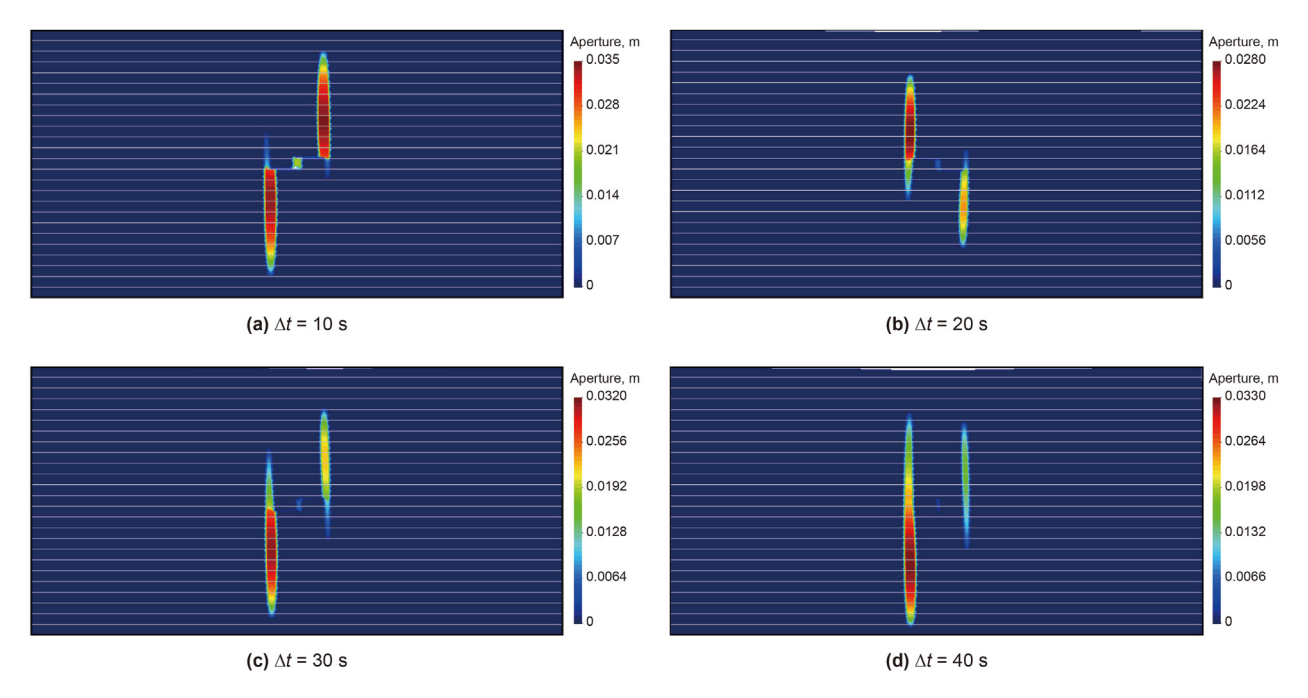


Fig. 16. Three-cluster fracture propagation behavior for fracturing sequence: Cluster 1 - Cluster 3 - Cluster 2.

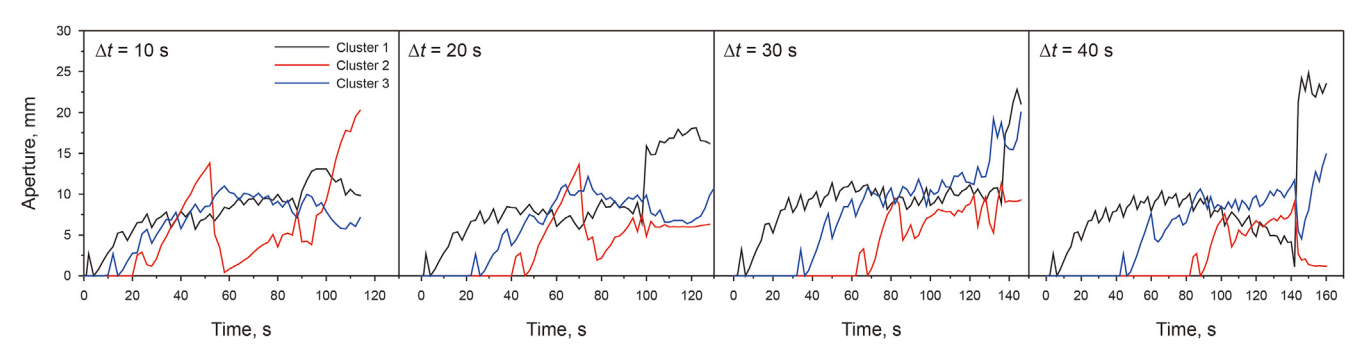
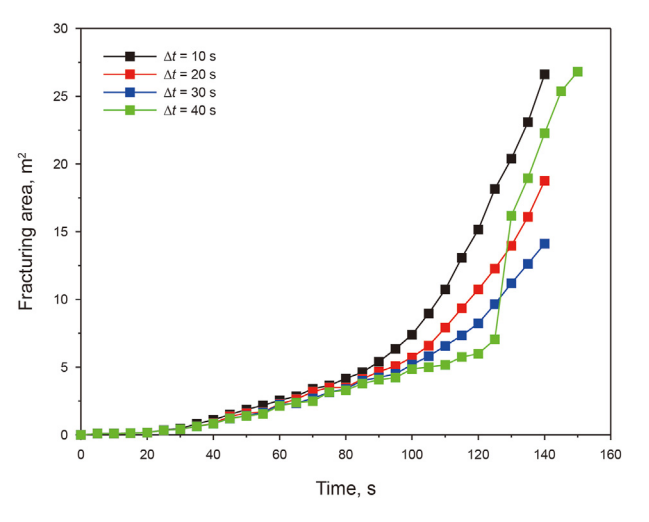


Fig. 17. Variations of fracture aperture with time for fracturing sequence: Cluster 1 - Cluster 3 - Cluster 2.



 $\begin{tabular}{ll} \textbf{Fig. 18.} & Variations of fracturing area with time for fracturing sequence: Cluster 1 - Cluster 2 - Cluster 3. \\ \end{tabular}$

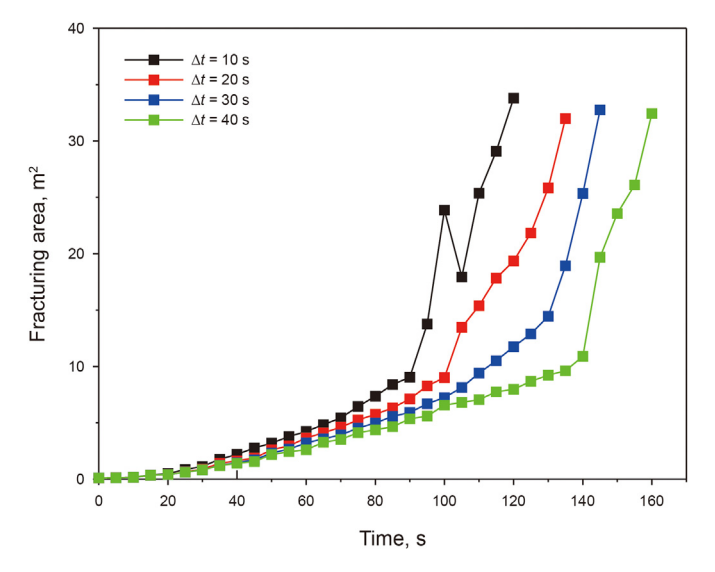


Fig. 19. Variations of fracturing area with time for fracturing sequence: Cluster 1 - Cluster 3 - Cluster 2.

4.2. Effect of alternative injection scheme

Previous studies have proposed that cyclic alternating fracturing and alternating shut-in fracturing could decrease the breakdown pressure and reduce the risk of induced seismicity (Patel et al., 2017; Zhuang et al., 2020; Liu et al., 2021). In this section, to discuss the effect of cyclic injection and shut-in injection on fracture morphology in shale with high-density bedding planes, we design three different alternative injection schemes, as displayed in Fig. 3. In the first scheme, the fracturing time for each cluster is 50 s. In the second scheme, the shut-in time lasts for 50 s and the fracturing time is the same as Scheme 1. In the last scheme, the single fracturing time for each cluster at each cycle is 20 s, and three cycles are conducted in the current simulation. The total fracturing time is same for the above fracturing scheme (total fracturing time is 100 s). In the above-mentioned scheme, the injection rate for Cluster 1 is equal to that of Cluster 2 ($q_1 = q_2 = 1 \times 10^{-4} \,\mathrm{m}^2/\mathrm{s}$). Nine clusters are simulated with the cluster spacing of 5 m.

The nine-cluster fracture morphologies for simultaneous injection and other three different alternative injection schemes are depicted in Fig. 20. It is observed that the alternative injection generally generates hydraulic fractures with smaller aperture compared with the simultaneous injection. Simultaneous injection facilitates to generate connected fractures with more bedding planes activated near the inter-cluster. The modified alternating fracturing and cyclic alternating fracturing enable the post fracturing cracks expanding towards the direction of pre-existing hydraulic fracture, and developing along the bedding planes. The length of the post fracturing cracks is inhibited by the existed fracturing cracks and the bedding planes. On the contrast, according to the results of alternating shut-in injection scheme, fivecluster fractures propagate vertically along maximum principal stress. During the shut-in time, the pressure at the crack tip maintains at a high value rather than decrease significantly, causing the fracture to continue expanding to propagate towards the vertical stress. The newly generated hydraulic fractures from Cluster 2 have larger aperture. It can be explained that the release of the pore pressure reduces the effect of stress interference, as well as Cluster

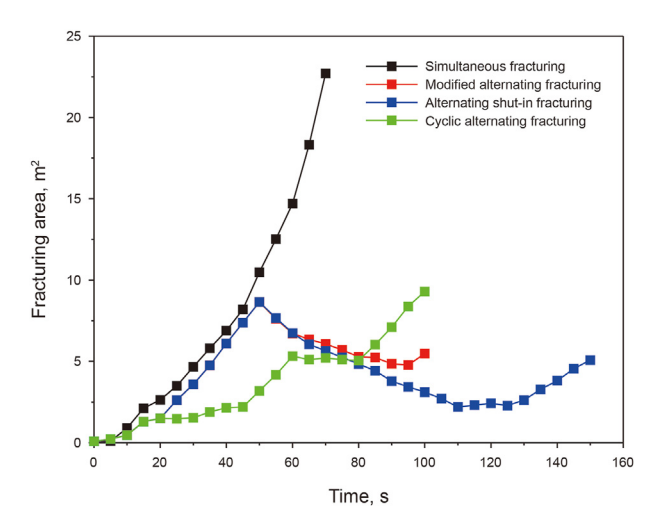


Fig. 21. Variations of fracturing area with time for different alternative injection schemes.

$1\ \ fractures$ are compressed by Cluster $2\ \ fractures$ without proppants.

Fig. 21 shows the fracturing area under nine clusters for simultaneous fracturing, modified alternating fracturing, alternating shut-in fracturing, and cyclic alternating fracturing. Simultaneous injection provides the most extensive area of stimulation, which is contributed by larger bedding plane slip displacements and wider hydraulic fracture aperture. When conducting alternative injection, cyclic alternating fracturing could achieve a better reservoir transformation with continuous vertical propagation of Cluster 1 and further bedding slipping and dilation induced by Cluster 2. For shut-in fracturing, more vertical main fractures could be obtained. However, it is noted, Xia et al. (2024) pointed that alternating shut-in fracturing benefits the increase in fracture length, and cyclic alternating fracturing facilitates uniform fracture propagation in homogeneous rock. This conclusion is not applicable

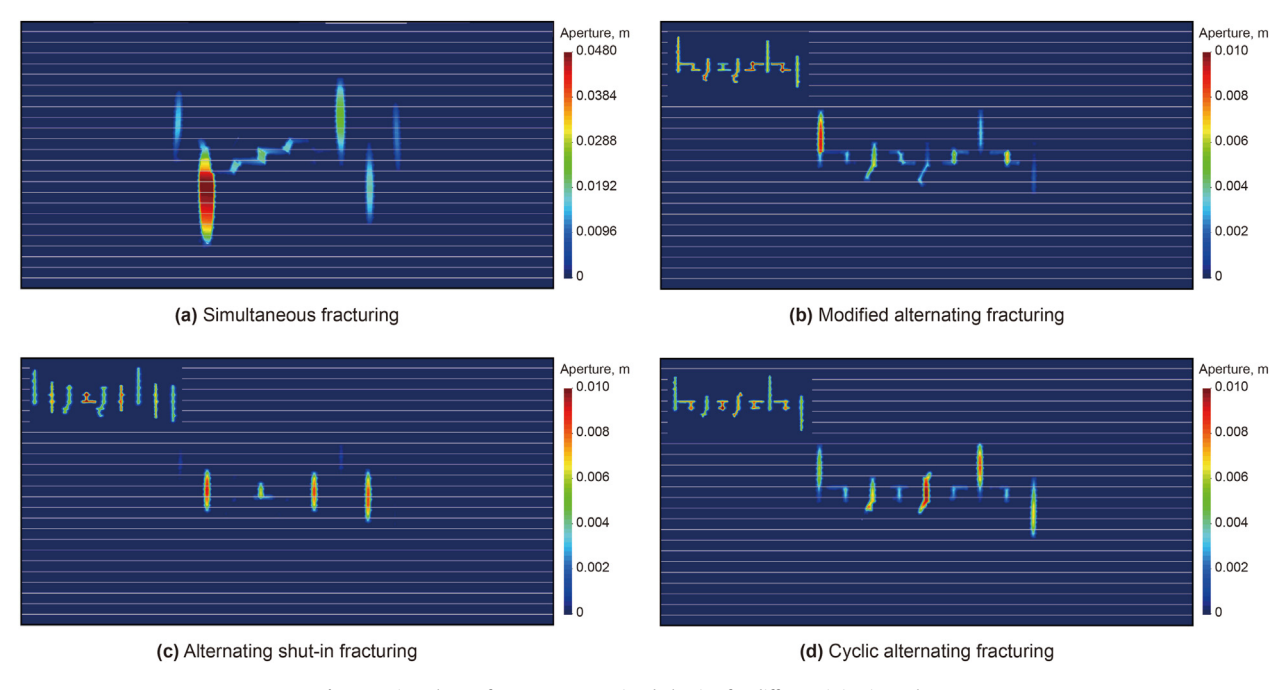


Fig. 20. Nine-cluster fracture propagation behavior for different injection schemes.

to the multi-cluster fracturing in layered shale with high-density bedding planes.

5. Conclusions

In this paper, UP-IEM is utilized to investigate the multi-cluster fracturing behavior and fracturing efficiency in high-density layered shale. This method incorporates the geo-mechanical effect, pressure diffusion in rock matrix, as well as the frictional slip and tensile failure of the bedding planes. The multi-cluster simultaneous fracturing, sequential fracturing, and alternative fracturing are conducted. The fracture morphology, fracture geometry, fracturing area, and multiple fracture propagation mechanism are analyzed. In addition, the effect of cluster spacing, injection rate, cluster number, interval time between each fracturing, and different injection schemes for alternating fracturing are discussed.

For simultaneous fracturing, the central fracture is easier to be arrested and then develops along the bedding planes under a small cluster spacing. The decrease in the cluster spacing results in a strong stress interference, further inducing uneven fracture aperture. Increasing the injection rate can effectively improve the fracturing efficiency by increasing the main fracture aperture, the slipping displacement and dilation of the bedding planes. With more cluster number, more bedding planes become activated, and the interior fractures mainly grow in the bedding planes. It is better to setting less cluster number to obtain more main fractures. For sequential fracturing and alternative fracturing, the propagation of post-fracturing cracks and the aperture of pre-existing fractures are affected by the combined action of the stress shadow and fluid pressure transfer through the bedding planes. Extending the interstage interval promotes the activation of additional bedding planes. The slipping and dilation of bedding planes restrict the vertical development of the subsequent fractures. The reactivation of the bedding planes can promote the extension of the fracturing area. For different alternative injection schemes, shut-in fracturing exhibits superiorities in creating main fractures along the direction of the maximum principal stress. To sum up, considering the sliding of the bedding planes, the fracturing area for multi-cluster simultaneous injection is the largest for shale reservoir with highdensity bedding planes, followed by the alternative injection and sequential injection.

CRediT authorship contribution statement

Xiao Yan: Writing — original draft, Validation, Software, Methodology, Funding acquisition, Formal analysis, Data curation. **Haitao Yu:** Writing — review & editing, Supervision, Resources, Project administration, Funding acquisition, Conceptualization. **Peng Zhang:** Visualization, Supervision, Resources, Investigation.

Declaration of competing interest

The authors declare that they have no known competing financial interests or personal relationships that could have appeared to influence the work reported in this paper.

Acknowledgements

The authors wish to acknowledge the financial support from Intergovernmental International Science and Technology Innovation Cooperation Key Project (2022YFE0128400), National Natural Science Foundation of China (42307209), Shanghai Pujiang Program (2022PJD076), State Energy Center for Shale Oil Research and Development (33550000-22-ZC0613-0365), and Natural Science Foundation of Qinghai Province (No. 2024-ZI-717).

References

- Barenblatt, G.I., 1962. The mathematical theory of equilibrium cracks in brittle fracture. Adv. Appl. Mech. https://doi.org/10.1016/S0065-2156(08)70121-2.
- Blanton, T.L., 1982. An experimental study of interaction between hydraulically induced and pre-existing fractures. In: SPE Unconventional Resources Conference/Gas Technology Symposium. https://doi.org/10.2118/10847-MS.
- Chang, X., 2019. Laboratory analysis of liquid injection method on hydraulic fracturing initiation and propagation in deep shale formation. Nat. Gas. Ind. B 6, 652–658. https://doi.org/10.1016/j.ngib.2019.11.001.
- Chang, X., Xu, E., Guo, Y., Yang, C., Hu, Z., Guo, W., 2022a. Experimental study of hydraulic fracture initiation and propagation in deep shale with different injection methods. J. Pet. Sci. Eng. 216, 110834. https://doi.org/10.1016/ i.petrol.2022.110834.
- Chang, Z., Hou, B., Ding, J., 2022b. Competitive propagation simulation of multiclustered fracturing in a cracked shale oil reservoir. Geomech. Geophys. Geo. Energy Ge Resour. 8. https://doi.org/10.1007/s40948-022-00399-x.
- Chen, M., Zhang, S., Xu, Y., Ma, X., Zou, Y., 2020. A numerical method for simulating planar 3D multi-fracture propagation in multi-stage fracturing of horizontal wells. Petrol. Explor. Dev. 47, 171–183. https://doi.org/10.1016/S1876-3804(20) 60016-7.
- Cheng, W., Jin, Y., Chen, M., Xu, T., Zhang, Y., Diao, C., 2014. A criterion for identifying hydraulic fractures crossing natural fractures in 3D space. Petrol. Explor. Dev. 41, 371–376. https://doi.org/10.1016/S1876-3804(14)60042-2.
- Dahi Taleghani, A., Gonzalez, M., Shojaei, A., 2016. Overview of numerical models for interactions between hydraulic fractures and natural fractures: challenges and limitations, Comput. Geotech. 71, 361–368. https://doi.org/10.1016/j.compgeo.2015.09.009.
- Dontsov, E., Suarez-Rivera, R., 2020. An equivalent representation of multiple hydraulic fractures with a fewer number of fractures. SPE J. 26, 293–306. https://doi.org/10.2118/202497-PA.
- Fang, Y., Elsworth, D., Wang, C., Ishibashi, T., Fitts, J.P., 2017. Frictional stability-permeability relationships for fractures in shales. J. Geophys. Res. Solid Earth 122, 1760–1776. https://doi.org/10.1002/2016JB013435.
- Guo, Q., Li, S., Jin, Z., Zhou, X., Liu, C., 2023. Characteristics and exploration targets of Chang 7 shale oil in Triassic Yanchang formation, Ordos Basin, NW China. Petrol. Explor. Dev. 50, 878–893. https://doi.org/10.1016/S1876-3804(23)60435-5.
- Huang, C., Zhu, H., Wang, J., Han, J., Zhou, G., Tang, X., 2022. A FEM-DFN model for the interaction and propagation of multi-cluster fractures during variable fluidviscosity injection in layered shale oil reservoir. Pet. Sci. 19, 2796–2809. https:// doi.org/10.1016/j.petsci.2022.06.007.
- Khisamitov, I., Meschke, G., 2021. Variational interface element model for 2D and 3D hydraulic fracturing simulations. Comput. Methods Appl. Mech. Eng. 373, 113450. https://doi.org/10.1016/j.cma.2020.113450.
- Kumar, D., Ghassemi, A., 2016. A three-dimensional analysis of simultaneous and sequential fracturing of horizontal wells. J. Pet. Sci. Eng. 146, 1006–1025. https://doi.org/10.1016/j.petrol.2016.07.001.
- Li, C.C., 2024. Field observations and interpretation of extensional fracture in hard rock surrounding deep underground openings. Deep Resour. Eng. 1, 100006. https://doi.org/10.1016/j.deepre.2024.100006.
- Li, Y., Chen, X., Zhao, J., Xu, W., Wu, J., Fu, D., 2018. Influence of perforation erosion on multiple growing hydraulic fractures in multi-stage fracturing. Nat. Gas. Ind. B 5, 8–15. https://doi.org/10.1016/j.ngib.2017.11.002.
- Li, Y., Zhu, Y., Li, Z., Jiang, T., Xue, Z., Shen, Z., Xiao, P., Yu, H., Cheng, Z., Zhao, Q., Zhang, Q., 2024. Shale oil recovery by CO₂ injection in Jiyang depression, Bohai Bay Basin, east China. Petrol. Explor. Dev. 51, 981–992. https://doi.org/10.1016/51876-3804(24)60519-7.
- Liu, D., Li, Z., Jiang, Z., Zhang, C., Zhang, Z., Wang, J., Yang, D., Song, Y., Luo, Q., 2019a. Impact of laminae on pore structures of lacustrine shales in the southern Songliao Basin, NE China. J. Asian Earth Sci. 182, 103935. https://doi.org/10.1016/ iiseaes 2019 103935
- Liu, X., Qu, Z., Guo, T., Sun, Y., Wang, Z., Bakhshi, E., 2019b. Numerical simulation of non-planar fracture propagation in multi-cluster fracturing with natural fractures based on Lattice methods. Eng. Fract. Mech. 220, 106625. https://doi.org/ 10.1016/j.engfracmech.2019.106625.
- Liu, H., Bao, Y., Zhang, S., Li, Z., Li, J., Wang, X., Wu, L., Wang, Y., Wang, W., Zhu, R., Zhang, S., Wang, X., 2023a. Structural characteristics of continental carbonaterich shale and shale oil movability: a case study of the Paleogene Shahejie Formation shale in Jiyang Depression, Bohai Bay Basin, China. Petrol. Explor. Dev. 50. 1320–1332. https://doi.org/10.1016/51876-3804/24)60469-6.
- Liu, H., Huang, Y., Cai, M., Meng, S., Tao, J., 2023b. Practice and development suggestions of hydraulic fracturing technology in the Gulong shale oil reservoirs of Songliao Basin, NE China. Petrol. Explor. Dev. 50, 688–698. https://doi.org/10.1016/S1876-3804(23)60420-3.
- Liu, J., Sheng, J.J., Emadibaladehi, H., Tu, J., 2021. Experimental study of the stimulating mechanism of shut-in after hydraulic fracturing in unconventional oil reservoirs. Fuel 300, 120982. https://doi.org/10.1016/j.fuel.2021.120982.
- Liu, W., Liu, H., Wang, S., Dong, K., 2023c. A multi-fracture balanced extension control method for horizontal wells in anisotropic shale. Eng. Fract. Mech. 281, 109102. https://doi.org/10.1016/j.engfracmech.2023.109102.
- Ma, X., Jiang, D., Fang, X., Wang, X., 2022. Numerical simulation of single-cluster and multi-cluster fracturing of hydrate reservoir based on cohesive element. Eng. Fract. Mech. 265, 108365. https://doi.org/10.1016/j.engfracmech.2022.108365.
- Manchanda, R., Bryant, E.C., Bhardwaj, P., Cardiff, P., Sharma, M.M., 2017. Strategies

for effective stimulation of multiple perforation clusters in horizontal wells. SPE Prod. Oper. 33, 539–556, https://doi.org/10.2118/179126-PA.

- Mei, Q., Guo, R., Zhou, X., Cheng, G., Li, S., Bai, Y., Liu, J., Wu, W., Zhao, J., 2023. Pore structure characteristics and impact factors of laminated shale oil reservoir in Chang 73 sub-member of Ordos Basin, China. J. Nat. Gas Geosci. 8, 227–243. https://doi.org/10.1016/j.jnggs.2023.07.003.
 Meng, S., Tao, J., Li, T., Li, D., Wang, S., Yang, L., Liu, X., Liang, L., Liu, H., 2024. Me-
- Meng, S., Tao, J., Li, T., Li, D., Wang, S., Yang, L., Liu, X., Liang, L., Liu, H., 2024. Mechanical characteristics and reservoir stimulation mechanisms of the Gulong shale oil reservoirs, the northern Songliao Basin. Pet. Sci. 21, 2023–2036. https://doi.org/10.1016/j.petsci.2023.11.002.
- Nguyen, V.P., Lian, H., Rabczuk, T., Bordas, S., 2017. Modelling hydraulic fractures in porous media using flow cohesive interface elements. Eng. Geol. 225, 68–82. https://doi.org/10.1016/j.enggeo.2017.04.010.
- Oliver, J., Huespe, A.E., Cante, J.C., 2008. An implicit/explicit integration scheme to increase computability of non-linear material and contact/friction problems. Comput. Methods Appl. Mech. Eng. 197, 1865—1889. https://doi.org/10.1016/j.cma.2007.11.027.
- Pan, P., Tan, F., Li, F., Chi, F., Liu, X., Wang, Z., 2024. A three-dimensional numerical study on the stability of layered rock spillway tunnels in alpine canyon areas. Deep Resour. Eng. 1, 100023. https://doi.org/10.1016/j.deepre.2024.100023.
- Patel, S.M., Sondergeld, C.H., Rai, C.S., 2017. Laboratory studies of hydraulic fracturing by cyclic injection. Int. J. Rock Mech. Min. Sci. 95, 8–15. https://doi.org/10.1016/j.ijrmms.2017.03.008.
- Qianli, L., Zhuang, L., Jianchun, G., Longqing, Z., Le, H., Lei, C., 2023. Numerical investigation of fracture interference effects on multi-fractures propagation in fractured shale. Eng. Fract. Mech. 286, 109322. https://doi.org/10.1016/ i.engfracmech.2023.109322.
- Remij, E.W., Remmers, J.J.C., Huyghe, J.M., Smeulders, D.M.J., 2015. The enhanced local pressure model for the accurate analysis of fluid pressure driven fracture in porous materials. Comput. Methods Appl. Mech. Eng. 286, 293–312. https:// doi.org/10.1016/j.cma.2014.12.025.
- Ren, X., Zhou, L., Li, H., Lu, Y., 2019. A three-dimensional numerical investigation of the propagation path of a two-cluster fracture system in horizontal wells. J. Pet. Sci. Eng. 173, 1222—1235. https://doi.org/10.1016/j.petrol.2018.10.105.
- Rutqvist, J., Wu, Y.S., Tsang, C.F., Bodvarsson, G., 2002. A modeling approach for analysis of coupled multiphase fluid flow, heat transfer, and deformation in fractured porous rock. Int. J. Rock Mech. Min. Sci. 39, 429–442. https://doi.org/ 10.1016/S1365-1609(02)00022-9.
- Saberhosseini, S.E., Ahangari, K., Mohammadrezaei, H., 2019. Optimization of the horizontal-well multiple hydraulic fracturing operation in a low-permeability carbonate reservoir using fully coupled XFEM model. Int. J. Rock Mech. Min. Sci. 114, 33–45. https://doi.org/10.1016/j.ijrmms.2018.09.007.
- Saeb, S., Amadei, B., 1992. Modelling rock joints under shear and normal loading. Int. J. Rock Mech. Min. Sci. Geomech. Abstracts 29, 267–278. https://doi.org/ 10.1016/0148-9062(92)93660-C.
- Sesetty, V., Ghassemi, A., 2013. Numerical simulation of sequential and simultaneous hydraulic fracturing. In: ISRM International Conference for Effective and Sustainable Hydraulic Fracturing.
- Shao, J., Yu, Z., Liu, Z., Vu, M., Armand, G., 2024. Numerical analysis of thermohydromechanical process related to deep geological radioactive repository. Deep Resour. Eng. 1 (1), 100001. https://doi.org/10.1016/j.deepre.2024.100001.
- Siddhamshetty, P., Wu, K., Kwon, J.S., 2018. Optimization of simultaneously propagating multiple fractures in hydraulic fracturing to achieve uniform growth using data-based model reduction. Chem. Eng. Res. Des. 136, 675–686. https://doi.org/10.1016/j.cherd.2018.06.015.
- Snozzi, L., Molinari, J.F., 2013. A cohesive element model for mixed mode loading with frictional contact capability. Int. J. Numer. Methods Eng. 93, 510–526. https://doi.org/10.1002/nme.4398.
- Sobhaniaragh, B., Mansur, W.J., Peters, F.C., 2018. The role of stress interference in hydraulic fracturing of horizontal wells. Int. J. Rock Mech. Min. Sci. 106, 153–164. https://doi.org/10.1016/j.ijrmms.2018.04.024.
- Sun, Z., Yan, X., Han, W., Ma, G., Zhang, Y., 2019. Simulating the filtration effects of

- cement-grout in fractured porous media with the 3D unified pipe-network method. Processes 7, 46. https://doi.org/10.3390/pr7010046.
- Tan, P., Jin, Y., Han, K., Hou, B., Chen, M., Guo, X., Gao, J., 2017. Analysis of hydraulic fracture initiation and vertical propagation behavior in laminated shale formation. Fuel 206, 482–493. https://doi.org/10.1016/j.fuel.2017.05.033.
- Tian, W., Li, P., Dong, Y., Lu, Z., Lu, D., 2019. Numerical simulation of sequential, alternate and modified zipper hydraulic fracturing in horizontal wells using XFEM. J. Pet. Sci. Eng. 183, 106251. https://doi.org/10.1016/j.petrol.2019.106251.
- Wang, X., Zhang, F., Tang, M., Du, X., Hou, B., Tang, J., 2023. Numerical investigation of hydraulic fracture deflection in large-angle oblique horizontal wells with staged multi-cluster fracturing. Geoenergy Sci. Eng. 222, 211436. https:// doi.org/10.1016/j.geoen.2023.211436.
- Wang, Y., Ju, Y., Zhang, H., Gong, S., Song, J., Li, Y., Chen, J., 2021. Adaptive finite element—discrete element analysis for the stress shadow effects and fracture interaction behaviours in three-dimensional multistage hydrofracturing considering varying perforation cluster spaces and fracturing scenarios of horizontal wells. Rock Mech. Rock Eng. 54, 1815—1839. https://doi.org/10.1007/s00603-021-02364-8.
- Wei, J., Zhang, A., Li, J., Shang, D., Zhou, X., 2023. Study on microscale pore structure and bedding fracture characteristics of shale oil reservoir. Energy 278, 127829. https://doi.org/10.1016/i.energy.2023.127829.
- Witherspoon, P.A., Wang, J.S.Y., Iwai, K., Gale, J.E., 1980. Validity of cubic law for fluid flow in a deformable rock fracture. Water Resour. Res. 16, 1016–1024. https://doi.org/10.1029/WR016i006p01016.
- Wu, K., Olson, J., Balhoff, M.T., Yu, W., 2016. Numerical analysis for promoting uniform development of simultaneous multiple-fracture propagation in horizontal wells. SPE Prod. Oper. 32, 41–50. https://doi.org/10.2118/174869-PA.
- Xia, Y., Yao, M., Li, T., Yang, H., Tang, C., 2024. Numerical analysis of hydraulic fracture propagation in deep shale reservoir with different injection strategies. J. Rock Mech. Geotech. Eng. 16, 3558–3574. https://doi.org/10.1016/ j.jrmge.2024.02.013.
- Yan, X., Yu, H., 2022. Numerical simulation of hydraulic fracturing with consideration of the pore pressure distribution based on the unified pipe-interface element model. Eng. Fract. Mech. 275, 108836. https://doi.org/10.1016/j.engfracmech.2022.108836.
- Yan, X., Sun, Z., Dong, Q., 2021. The unified pipe-interface element method for simulating the coupled hydro-mechanical grouting process in fractured rock with fracture propagation. Eng. Fract. Mech. 256, 107993. https://doi.org/ 10.1016/j.engfracmech.2021.107993.
- Yan, X., Yu, H., Jing, H., 2024. Numerical investigation of the stress regime effect on injection-induced fault reactivation and associated seismicity. Comput. Geotech. 169, 106251. https://doi.org/10.1016/j.compgeo.2024.106251.
- Yang, C., Yi, L., Yang, Z., Li, X., 2022. Numerical investigation of the fracture network morphology in multi-cluster hydraulic fracturing of horizontal wells: a DDM-FVM study. J. Pet. Sci. Eng. 215, 110723. https://doi.org/10.1016/ j.petrol.2022.110723.
- Yang, Z., Yi, L., Li, X., He, W., 2018. Pseudo-three-dimensional numerical model and investigation of multi-cluster fracturing within a stage in a horizontal well. J. Pet. Sci. Eng. 162, 190–213. https://doi.org/10.1016/j.petrol.2017.12.034.
- Zangeneh, N., Eberhardt, E., Bustin, R.M., 2015. Investigation of the influence of stress shadows on horizontal hydraulic fractures from adjacent lateral wells.
 J. Unconvent. Oil Gas Resour. 9, 54–64. https://doi.org/10.1016/j.juogr.2014.11.001.
- Zhou, J., Chen, M., Jin, Y., Zhang, G., 2008. Analysis of fracture propagation behavior and fracture geometry using a tri-axial fracturing system in naturally fractured reservoirs. Int. J. Rock Mech. Min. Sci. 45 (7), 1143–1152. https://doi.org/10.1016/ j.ijrmms.2008.01.001.
- Zhuang, L., Jung, S.G., Diaz, M., Kim, K.Y., Hofmann, H., Min, K., Zang, A., Stephansson, O., Zimmermann, G., Yoon, J., 2020. Laboratory true triaxial hydraulic fracturing of granite under six fluid injection schemes and grain-scale fracture observations. Rock Mech. Rock Eng. 53, 4329–4344. https://doi.org/10.1007/s00603-020-02170-8.